

Development of Compact Muon Spectrometer Using Multiple Pressurized Gas Cherenkov Radiators

Junghyun Bae^{1,*} and Stylianos Chatzidakis¹

¹ School of Nuclear Engineering, Purdue University, IN 47906

bae43@purdue.edu, schatzid@purdue.edu

Abstract

In both particle physics and muon applications, a high-resolution muon momentum measurement capability plays a significant role not only in providing valuable information on the properties of subatomic particles but also in improving the utilizability of cosmic ray muons. Typically, muon momentum is measured by reconstructing a curved muon path using a strong magnetic field and muon trackers. Alternatively, a time-of-flight and Cherenkov ring imager are less frequently applied, especially when there is a need to avoid a magnetic field. However, measurement resolution is much less than that of magnetic spectrometers, approximately 20% whereas it is nearly 4% or less when using magnets and trackers. Here, we propose a different paradigm to estimate muon momentum that utilizes multiple pressurized gas Cherenkov radiators. Using the fact that the refractive index of gas medium varies depending on its pressure and temperature, we can optimize the muon Cherenkov threshold momentum levels for which a muon signal will be detected. In this work, we demonstrate that muon momentum can be estimated with mean resolution of $\sigma_p/p < 20\%$ and mean classification rate of 90.08% in the momentum range of 0.1 to 10.0 GeV/c by analyzing optical photon signals from each Cherenkov radiator. We anticipate our new spectrometer will significantly improve quality of imaging and reduce scanning time in cosmic ray muon applications by being incorporated with existing instruments.

Keywords – Cosmic ray muons, Radiation instrumentation, Cherenkov radiation, Spectrometer, Muon momentum

*Corresponding author
Email: bae43@purdue.edu

1. Introduction

Muons are one of the most versatile particles in both particle physics and nuclear engineering. Not only are muons the key particles in accelerator and neutrino studies, e.g., CMS and miniBooNE [1,2], but also a promising non-conventional radiographic probe in muon applications, e.g., nuclear reactor and waste imaging [3–7], homeland security [8–14], geotomography [15–19], and archeology [20,21]. In particle physics, two important quantities, muon trajectory and momentum, need to be measured. Typically, muon trackers and a combination of strong magnets are used to reconstruct muon trajectories and measure muon momentum, respectively [22]. In certain cases where application of a strong magnetic field is not practical, a time-of-flight or Cherenkov ring imager is used to measure muon momentum [23]. However, the average measurement resolution is much lower than that of magnetic spectrometers, ~20% or worse [24].

When it comes to muon tomography, or muography, the imaging resolution is often limited by the naturally low muon flux, approximately $7.25 \pm 0.1 \text{ cm}^{-2}\text{s}^{-1}\text{sr}^{-1}$ at sea level [25]. In addition, muon flux varies with zenith angle and detector configuration [26,27]. Incorporating additional information such as muon momentum has potential to maximize and expand utilizability of cosmic ray muons to various engineering applications. Despite the apparent benefits [28,29], it is still very challenging to measure muon momentum in the field without deploying large and expensive spectrometers. Existing spectrometers are not well suited for muon tomographic applications that demand portability, limited available space, small size requirements, and minimal cost. Additional challenges with existing spectrometers include interference with muon traveling path (mostly a problem for magnetic spectrometers), a vast array of detectors, e.g., Ring Image Cherenkov Detector, or a very long line of sight (for time-of-flight spectrometers). At present, neither fieldable nor portable muon spectrometers exist.

In this work, we present a different paradigm for muon momentum measurement using multiple pressurized gas Cherenkov radiators. By carefully selecting gas pressure at each radiator, we can optimize muon Cherenkov momentum threshold for which a muon signal will be detected. In this design, a muon passing through all radiators will activate only those that have a threshold momentum level less than actual muon momentum. By measuring the presence of Cherenkov radiation signals in each radiator, we can estimate the muon momentum with absolute resolution of $\pm 0.5 \text{ GeV}/c$ using six Cherenkov radiators over the muon momentum range of 0.1 to 10.0 GeV/c . In addition, the dimension of our proposed spectrometer is smaller than 1 m which renders it easily transportable for field measurements. The primary benefits of our concept are: (i) it offers a versatile and portable muon spectrometer that provides similar or better resolution with existing spectrometers, (ii) it extends the measurable momentum range without relying on bulky and expensive magnetic spectrometers, and (iii) it provides a solution to muon momentum measurement in the field that is needed for various engineering applications, e.g., archaeology, geotomography, cosmic radiation measurements in the International Space Station, off-site particle experiment laboratories, nuclear safeguards, and non-destructive monitoring techniques.

2. Design and concept of Cherenkov muon spectrometer

To develop a compact Cherenkov muon spectrometer, we use multiple pressurized gas Cherenkov radiators with different refractive indices. We carefully select the refractive index of each radiator by varying the gas pressure to achieve the necessary Cherenkov threshold muon momentum. Muon momentum measurement resolution is determined by the maximum threshold momentum level and the number of

radiators. A fine resolution can be obtained by increasing the number of radiators in a given measurable muon momentum range. The absolute momentum measurement resolution, σ_p , is written by:

$$\Delta p_{th} = \frac{p_{th,max}}{N_{rad} - 1} \quad (1)$$

$$\sigma_p = \pm \Delta p_{th} / 2 \quad (2)$$

where N_{rad} is the number of radiators. Δp_{th} and $p_{th,max}$ are the interval and maximum threshold momentum, respectively. When the actual muon momentum is p_μ , muon momentum can be estimated using:

$$\hat{p}_\mu = (N_i - 1)\Delta p_{th} + \sigma_p \quad (3)$$

where N_i is the largest radiator number that emits Cherenkov radiation when $i = 1, 2, \dots, N_{rad}$. For our prototype design, we used six radiators, comprising of a glass (SiO₂) and five pressurized gas radiators (CO₂) with linearly increasing threshold momentum levels, $p_{th} = 0.1, 1.0, 2.0, 3.0, 4.0,$ and 5.0 GeV/c. The maximum momentum level is limited to 10.0 GeV/c because approximately 84% of cosmic ray muons have momentum less than 10.0 GeV/c as shown in Fig. 1. CO₂ is chosen as a gas radiator because it allows to be pressurized up to nearly 5.7 MPa and can cover a wide range of momentum threshold levels. The lowest momentum threshold radiator is replaced by SiO₂ because the threshold of 0.1 GeV/c is not possible to achieve using high-pressure CO₂ gas. Each radiator is designed to be triggered when a muon has at least momentum higher than a pre-selected level in that particular radiator. In other words, depending on the muon momentum, none to all Cherenkov radiators can be triggered. An overview of measuring muon momentum of $\sigma_p = \pm 0.5$ GeV/c using six Cherenkov radiators (one SiO₂ and five CO₂ gases) is illustrated in Fig. 2.

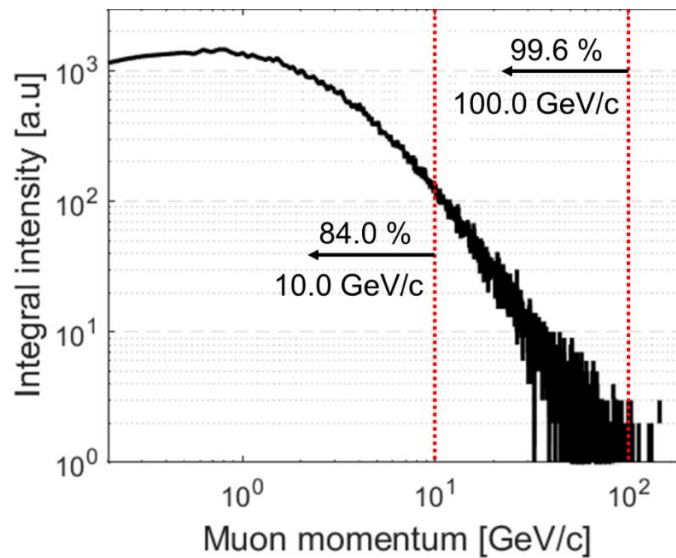


Fig. 1. Approximate fraction of muons within the cosmic ray muon spectrum.

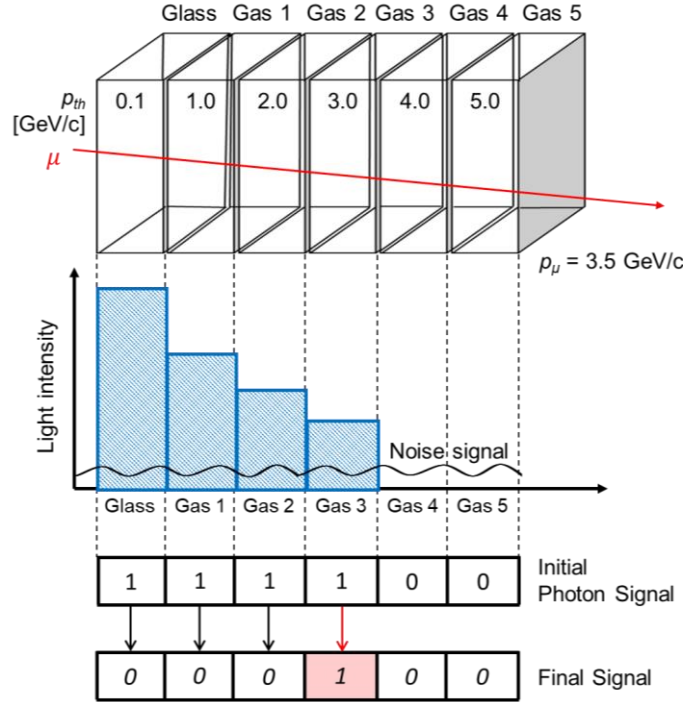


Fig. 2. Overview of measuring muon momentum with a resolution, $\sigma_p = \pm 0.5$ GeV/c using six Cherenkov radiators, one solid (SiO_2) and five gas (CO_2) radiators. Light intensity decreases as threshold momentum level increases because it depends on the refractive index of radiator. When Cherenkov radiation signals are detected in the radiator, it records “1” otherwise “0”. Subtracting the recorded signals allows identification of the radiator with the highest momentum threshold and classification of the muon momentum within a predetermined momentum range. For example, if a muon with actual momentum 3.5 GeV/c passes through the radiators, the muon spectrometer will assign this muon in the muon momentum range $3.0 < p_\mu (\text{GeV}/c) < 4.0$ estimating its momentum as 3.5 GeV/c [30].

2.1. Selection of gas radiators

To utilize gas Cherenkov radiators in our proposed Cherenkov spectrometer, we rely on two theories in physics: (i) Cherenkov effect and (ii) Lorentz-Lorenz equation [31,32]. When the velocity of a muon exceeds the speed of light in an optically transparent medium, or a radiator, Cherenkov radiation is emitted. This happens when the following criterion is satisfied:

$$\beta_\mu n > 1, \quad (4)$$

where β_μ is the ratio of the velocity of muon in the radiator to that of light in a vacuum ($= v_\mu/c$) and n is the refractive index of the radiator. As shown in Eq. (4), a minimum muon velocity is required so that Cherenkov light is emitted in a given radiator. A threshold momentum for muons can be derived as [33]:

$$p_{th}c = \frac{m_\mu c^2}{\sqrt{n^2 - 1}}, \quad (5)$$

where p_{th} is the threshold muon momentum and $m_\mu c^2$ represents the muon rest mass energy ($\cong 105.66$ MeV). From Eq. (5), we can see that the muon threshold momentum can be adjusted by properly selecting the refractive index of radiator. For a gas medium, the refractive index of gas varies depending on both pressure

and temperature. When $n^2 \approx 1$, the refractive index of gas radiator can be approximated by Lorentz-Lorenz equation:

$$n \approx \sqrt{1 + \frac{3A_m p}{RT}}, \quad (6)$$

where A_m is the molar refractivity, p is the gas pressure, T is the absolute temperature, and R is the universal gas constant. By substituting Eq. (6) into Eq. (5), Cherenkov threshold momentum for muons in terms of both gas pressure and temperature can be written as:

$$p_{th} c = m_\mu c^2 \sqrt{\frac{R T}{3A_m p}} \quad (7)$$

From Eq. (7), it can be seen that a threshold momentum is proportional to $p^{-1/2}$. As a result, by changing gas pressure, the threshold momentum can be changed without the need to replace any materials. The variation of Cherenkov threshold muon momentum, p_{th} , and the refractive index, n , as a function of gas pressure for four radiators, C_3F_8 , $C_3H_2F_4$ (R1234yf), C_4F_{10} , and CO_2 is shown in Fig. 3. We vary the gas pressure with maintaining at room temperature because (i) changing pressure covers a wider p_{th} range over that of temperature and (ii) maintaining high-pressure is more practical than keeping very low gas temperature in the field. Properties of gas Cherenkov radiators are summarized in Table I. C_4F_{10} and CO_2 have been used as gas Cherenkov radiators in the Jefferson Lab [34]. A refrigerant, R1234yf, is a promising substitute radiator to replace R12 (CCl_2F_2) due to its lower Ozone Depletion Potential (ODP) [35]. C_3F_8 is alternative to C_4F_{10} because C_4F_{10} cannot be pressurized higher than 380 kPa without condensation at room temperature. Based on the results from Fig. 3 and Table I, we chose CO_2 gas as our Cherenkov gas radiator because it covers a wide range of threshold momentum and it is commercially available in a large quantity at minimal cost. C_3F_8 would be also be a good candidate but it has a smaller vapor pressure and is more expensive.

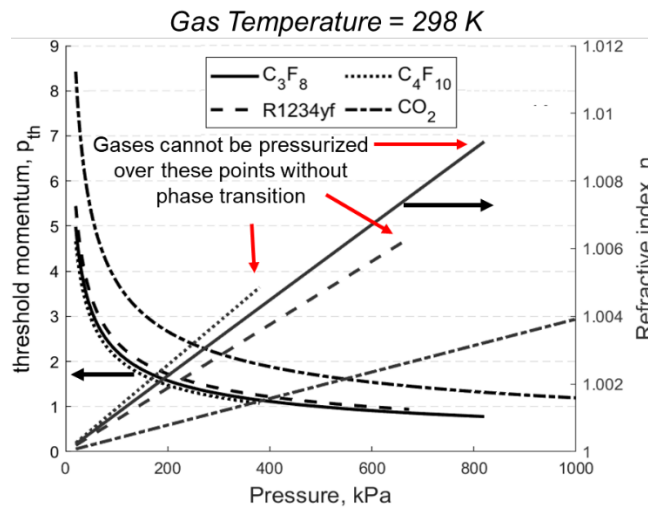


Fig. 3. Cherenkov threshold muon momentum (left) and refractive index (right) for C₃F₈, R1234yf, C₄F₁₀, and CO₂ gas radiators as a function of gas pressure. Note: gases cannot be pressurized above their vapor pressure without condensation.

Table 1

Material properties for selected Cherenkov gas radiators at room temperature [35–37].

Selected gas radiators	C ₃ F ₈	R1234yf	C ₄ F ₁₀	CO ₂
Vapor pressure [MPa]	0.820	0.673	0.380	5.7
Vapor density [kg/m ³]	12.5	37.6	24.6	1.977
Molecular weight [g/mol]	188.02	114.04	236.03	44.01
Refractive index [–]	1.0011	1.0010	1.0015	1.00045
Polarizability, α [$\times 10^{-30}$ m ³]	7.4	6.2	8.44	2.59

2.2. Cherenkov radiation

Typically, there are three predominant photon emission mechanisms when muons interact with optically transparent medium: (i) Cherenkov radiation, (ii) scintillation, and (iii) transition radiation [38]. Cherenkov photon intensity depends on various factors, refractive index, particle velocity, and path length. Expression for Cherenkov photon intensity was first derived by I. Frank and I. Tamm [39]. According to the Frank-Tamm formula, the expected number of Cherenkov photons in unit path length, dN_{ch}/dx , between wavelength, λ_1 and λ_2 , within a spectral region is given by:

$$\frac{dN_{ch}}{dx} = 2\pi\alpha \int_{\lambda_1}^{\lambda_2} \left(1 - \frac{1}{n^2(\lambda)\beta^2}\right) \frac{d\lambda}{\lambda^2} \quad (8)$$

where α is the fine structure constant ($\cong 1/137$), β is the muon phase velocity, and $n(\lambda)$ is the refractive index of gas radiator. When electromagnetic wavelength range is limited to optical photons (200–700 nm), Eq. (8) is simplified by:

$$\frac{dN_{ch}}{dx} \cong 1150 \sin^2 \theta_c \quad (9)$$

$$\theta_c = \cos^{-1} \left(\frac{1}{\beta n} \right), \quad (10)$$

where θ_c is the Cherenkov angle.

Cherenkov photon emission is the result of instant physical disorder caused by a charged particle such as a muon. Estimated duration of Cherenkov light flash, Δt is given by [40,41]:

$$\Delta t = \frac{r}{\beta c} \sqrt{\beta^2 n(\lambda) - 1} \Big|_{\lambda_1}^{\lambda_2}, \quad (11)$$

where r is the distance to the observer. Calculated Cherenkov light flash duration for a high-energy muon is less than a nanosecond as shown in Fig. 4.

2.3. Scintillation

When a portion of muon energy is transferred to the medium, molecules and atoms are excited against one another. The excitation energy is then released as a form of light which is called scintillation, when they return to the ground state. Wavelength of scintillation photon is extended approximately between 200 and 700 nm depending on types of scintillation medium [42]. Light yield of scintillation depends on muon energy deposited in the radiators. The mean number of scintillation photons per unit distance, dN_{sc}/dx , is given by [43]:

$$\frac{dN_{sc}}{dx} = S \frac{dE/dx}{1 + k_B(dE/dx)}, \quad (12)$$

where S is the scintillation efficiency, k_B is the Birks' coefficient, and dE/dx is the muon mass stopping power which can be calculated using the Bethe equation [44]. When the scintillation medium is gaseous state and $E \geq 300$ keV, then $k_B \approx 0$.

Unlike Cherenkov radiation, light flash duration of scintillation is associated with photon absorption, excitation, and relaxation. The time response of the prompt fluorescence of scintillation is given by [45]:

$$I/I_0 = f(t)e^{-t/\tau} \quad (13)$$

where I/I_0 is the normalized light intensity, $f(t)$ represents the characteristic Gaussian function, and τ is the time constant describing decay. The scintillation light flash duration is mainly determined by a decay constant which is order of μsec for inorganic and few $nsec$ for organic scintillation materials [42]. Estimated flash time responses and electromagnetic wavelength spectra for both Cherenkov and scintillation are shown in Fig. 4. Scintillation photons can be systematically discriminated from Cherenkov photons using two methods: differences in (i) light flash timing and (ii) light emission spectrum. A significant timing difference is observed between scintillation and Cherenkov radiation and they can be separated using a fast and fine timing resolution [46] as shown in Fig. 4 (left). In addition, given that scintillation and Cherenkov radiation are emitted in a homogeneous material, their spectra are distinguishable and most scintillation photons can be filtered out by selectively choosing either a UV photodiode detector or IR photovoltaic detector as shown in Fig. 4 (right).

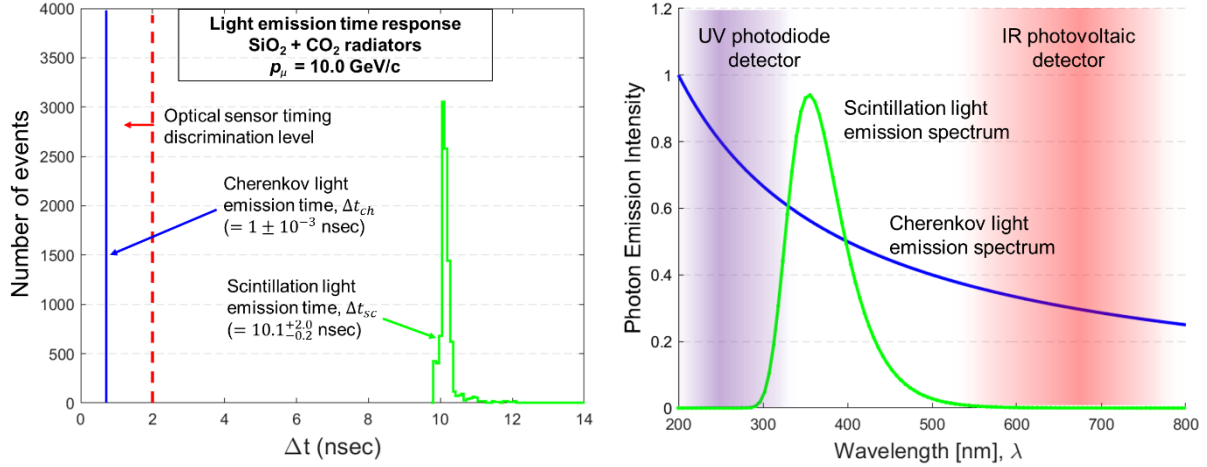


Fig. 4. Light emission time responses from Geant4 simulations for Cherenkov radiation and scintillation in SiO₂ and CO₂ radiators (left) and typical spectra of Cherenkov radiation and scintillation (right) [47]. Examples of sensitive EM wavelength for both UV photodiode and IR photovoltaic detectors to selectively detect Cherenkov radiation are also presented (right).

2.4. Transition radiation

When a muon passes through inhomogeneous media such as a boundary between two radiators, photons are emitted and they are called transition radiation. Transition radiation is sometimes misinterpreted as Cherenkov radiation because both have directional photon emission as shown in Fig. 5. However, transition radiation is neither related to particle energy loss by collisions at boundaries nor deceleration of muons. Especially, transition radiation that emits photons with a visible wavelength is called optical transition radiation (OTR) and a mean yield of OTR, when $\gamma \gg 1$ is given by [48]:

$$N_{tr} = \frac{z^2 \alpha}{\pi} \left[(\ln \gamma - 1)^2 + \frac{\pi^2}{12} \right], \quad (14)$$

where z is the muon charge, α is the fine structure constant, and γ is the Lorentz factor. Expected optical photon intensity is not significant ($10^{-3} \sim 10^{-4}$) when the number of physical boundaries is small and momentum range is not greater than 10 GeV/c [49].

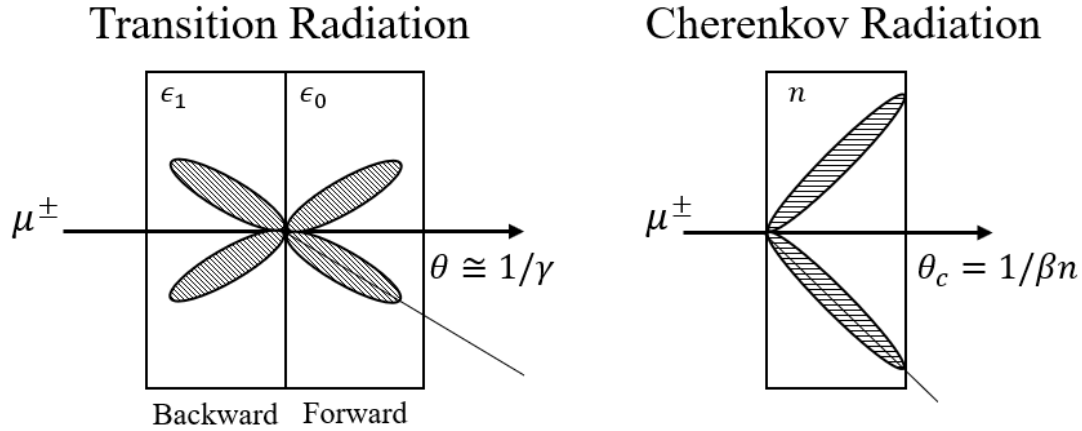


Fig. 5. Characteristics of transition and Cherenkov radiation when a muon passes through the media (photon emission angles are exaggerated) [50].

2.5. Optical photon emission in a gas radiator

Within each radiator, Cherenkov radiation, scintillation, and transition radiation can be emitted depending on conditions of muons and radiators. When incident muon momentum exceeds a threshold momentum, Cherenkov photons are expected to be emitted along a muon traveling path with a characteristic angle, or Cherenkov angle, θ_c . On the other hand, scintillation and transition photons can be emitted regardless of incoming muon momentum. Characteristics of photon emissions by Cherenkov radiation, scintillation, and transition radiation in both gas radiator A ($p_\mu > p_{th}$) and B ($p_\mu < p_{th}$) are shown in Fig. 6.

Expected optical photon yields by Cherenkov, scintillation, and transition radiation and Signal-to-Noise Ratio (SNR), $N_{ch}/(N_{sc}+N_{tr})$, as a function of radiator length for pressurized CO_2 and C_3F_8 are shown in Fig. 7. It appears that Cherenkov light emission yield increases more rapidly than that of scintillation. This means that to achieve a higher SNR, a large gas radiator would be preferable. In addition, the expected number of optical photons by transition radiation is negligible.

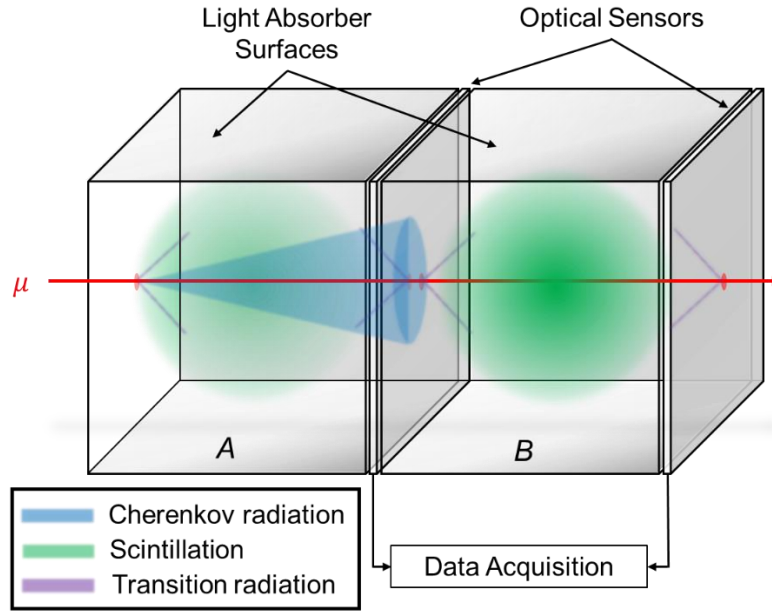


Fig. 6. Characteristics of light emission by Cherenkov radiation, scintillation, and transition radiation in two radiators. Radiator A (left) emits Cherenkov photons since $p_\mu > p_{th}$ whereas radiator B (right) does not because $p_\mu < p_{th}$. All surfaces of radiator containers are covered by light absorber except one in which optical sensors are placed. It is noted that the Cherenkov and transition radiation have characteristic directional light emission whereas scintillation light uniformly emits in all directions.

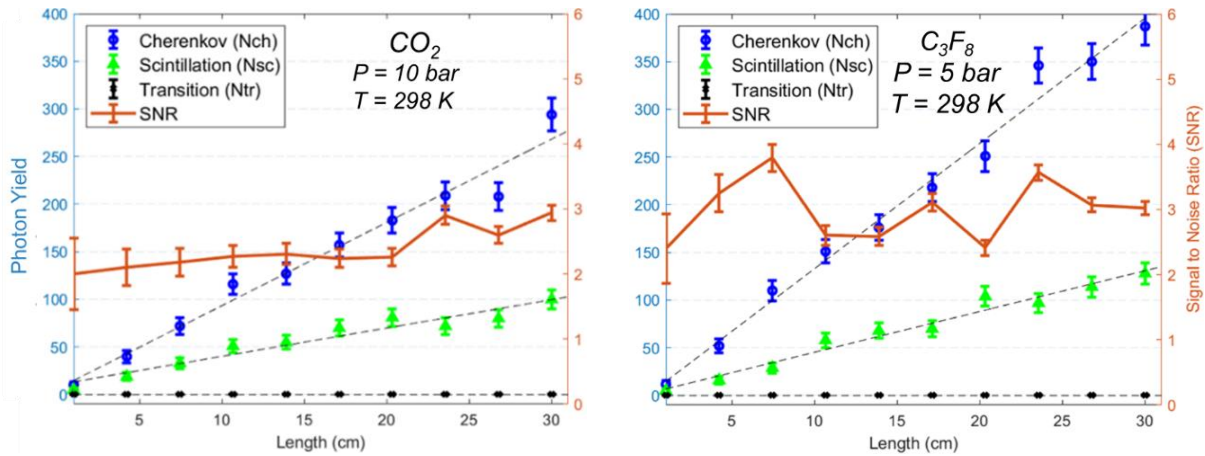


Fig. 7. Expected photon emission intensities by Cherenkov radiation, scintillation, and transition radiation when $p_\mu = 4.0 \text{ GeV}/c$ as a function of length in two pressurized gas radiators, CO_2 (left) and C_3F_8 (right). They show that Cherenkov light emission yield increases rapidly than those of scintillation and transition radiation. Error bars represent 1σ .

3. Geant4 Modeling

3.1. Geometry and materials

Geant4 (Geometry ANd Tracking) is a computational tool developed by CERN for Monte-Carlo particle transport simulations in many applications such as high-energy, nuclear, accelerator, medical, and space physics [51,52]. We used Geant4 to simulate muon interactions with matter, secondary particle production, scattering, absorption, and light emission in our proposed Cherenkov muon spectrometer. A surface area of radiators is $20 \times 20 \text{ cm}^2$ and gas radiators are enclosed by an aluminum housing with a thickness of 1 cm. Length of a glass radiator (SiO_2) is 1 cm, gas radiators are 10 cm each, and the aluminum photon absorber is 1 mm. All radiators and absorbers are included in the “world” volume which is made of air. Five pressurized CO_2 gas radiators are placed next to a solid radiator side by side. Each radiator chamber includes pressurized CO_2 gas to provide a pre-selected refractive index. Some CO_2 gas radiators are depressurized to achieve $p_{th} = 4$ and 5 GeV/c because Cherenkov threshold momentum for muon at atmospheric pressure is 3.52 GeV/c. Main parameters used in simulations for solid and gas radiators are summarized in Table II. Aluminum is added to simulate a strong photon absorber. Once optical photons arrive at the absorber surface, all disappear.

Table 2

Properties and parameters of materials used in Geant4 simulations.

Radiator ID	1	2	3	4	5	6	Absorber
Material	SiO_2	CO_2	CO_2	CO_2	CO_2	CO_2	Al
$\langle Z/A \rangle$ [-]	0.4973	0.4999	0.4999	0.4999	0.4999	0.4999	0.4818
Length [cm]	1	10	10	10	10	10	0.1
p_{th} [GeV/c]	0.1	1.0	2.0	3.0	4.0	5.0	-
Refractive index [-]	1.45	1.00557	1.00139	1.00062	1.00035	1.00022	-
Pressure [bar]	-	14.4857	3.6214	1.6095	0.9054	0.5794	-
Density [kg/m^3]	2500	27.83	6.55	2.88	1.61	1.03	2700
Radiation Length [cm]	10.69	1.93E4	1.96E4	1.96E4	1.97E4	1.97E4	8.90

3.2. Cosmic ray muons and physics list

All muons were initially generated 10 cm away from the center of solid radiator surface. All major physics, i.e., three optical photon emission mechanisms by both primary muons and secondary particles, scattering and absorption, decays, energy loss, are included in Geant4 reference physics list, QGSP_BERT [38]. All optical photons are accordingly tagged by types of mother particle (primary muon or secondary particle) and light emission mechanisms (Cherenkov, scintillation, and transition radiation).

4. Analytical model benchmarking

To verify our Geant4 model, we performed two benchmarking simulations: cosmic ray muon (i) scattering displacement distribution and (ii) energy loss. Analytical models for these benchmarking

examples were successfully developed based on multiple Coulomb scattering (MCS) and Bethe equation, respectively.

4.1. Scattering angle distribution

When a muon travels through matter, it is randomly deflected due to Coulomb interactions with atomic nuclei and electrons. The result of MCS is approximated using Gaussian distribution and its root mean square (rms) is derived by Highland [53].

$$f(\theta|0, \sigma_\theta^2) = \frac{1}{\sqrt{2\pi}\sigma_\theta} e^{-\theta^2/2\sigma_\theta^2} \quad (15)$$

$$\sigma_\theta = \frac{13.6 \text{ MeV}}{\beta c p} \sqrt{\frac{X}{X_0}} \left[1 + 0.088 \log_{10} \left(\frac{X}{X_0} \right) \right], \quad (16)$$

where θ and σ_θ are cosmic ray muon scattering angle and rms of scattering angle, respectively. X_0 is the radiation length and X is the length of the scattering medium. When a muon travels in inhomogeneous materials, the effective radiation length is given by:

$$\frac{X_{total}\rho_e}{X_{0,e}} = \sum_i \frac{X_i\rho_i}{X_{0,i}} \quad (17)$$

where X_{total} is the total length, ρ_e is the effective density of materials. X_i , $X_{0,i}$ and, ρ_i are the length, radiation length, and density of i^{th} material component. All parameters used to compute effective radiation length, $X_{0,e}$ are summarized in Table II. In addition, the rms of plane displacement of muons, σ_{plane} is related to σ_θ :

$$\sigma_{plane} = X\sigma_\theta \quad (18)$$

The analytical calculation of muon displacement is shown as a circle centered at the origin (initial muon x-y coordinate). The estimated radii (1σ , 2σ , and 3σ) of muon scattering displacement distributions for selected muon energies, 0.5, 1.0, 4.0, and 10.0 GeV, and Geant4 simulations are in good agreement and the results are shown in Fig. 8.

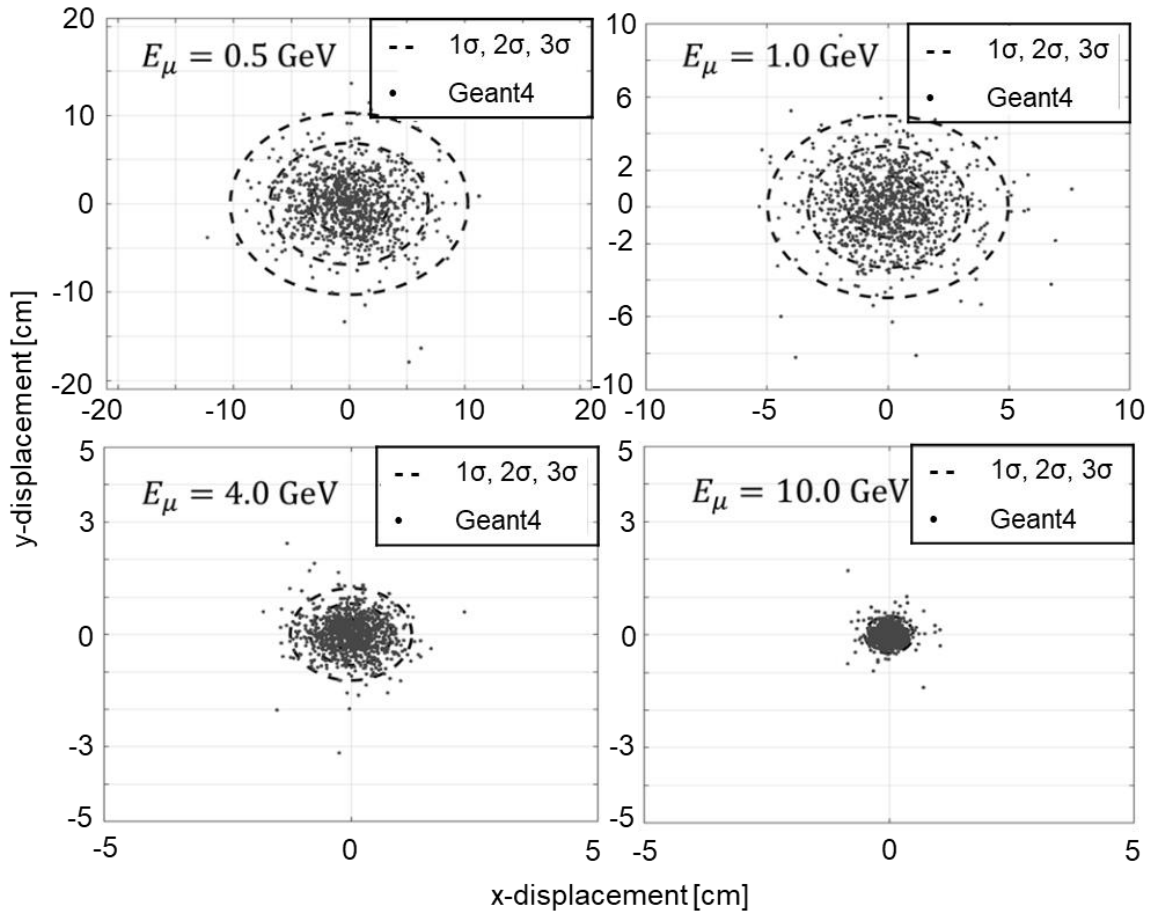


Fig. 8. The results of muon scattering displacement distributions in Geant4 simulations and analytical estimation using MCS Gaussian approximation. Each projected Gaussian circle (2D Gaussian distribution) represents 1σ (inner), 2σ (middle), and 3σ (outer). 99% of simulated muons are enclosed in the 3σ Gaussian circle. It is noted that different range of x- and y-axes are used.

4.2. Energy loss

Since muon energy loss by ionization dominates in most cosmic ray muon energy range (0.1 to 100 GeV/c), a mean muon mass stopping power can be estimated by using Bethe equation [54]. Fig. 9 shows Geant4 simulation results of muon energy loss in radiators as a function of muon energy using 10^4 muon samples. Even though the amount of muon energy loss varies slightly from 7 to 12 MeV depending on muon energy, a fraction of energy loss to initial muon energy is insignificant, $< 1\%$. The results from Geant4 simulations and analytical estimations using Bethe equation are in good agreement with each other.

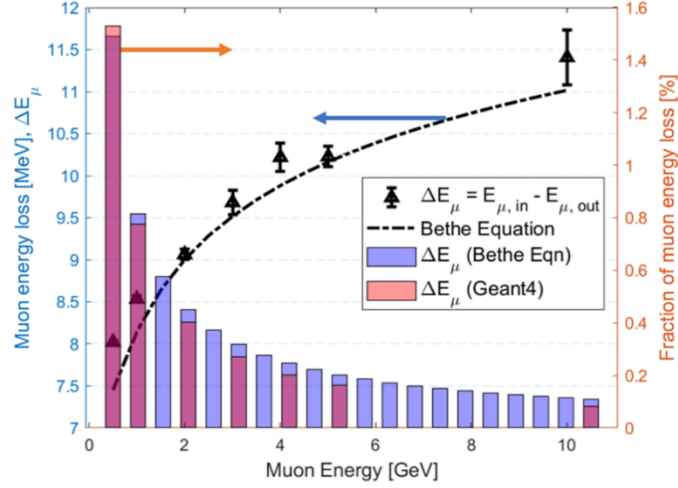


Fig. 9. Estimated cosmic ray muon energy loss using Bethe equation and Geant4 simulations using 10^4 muon samples (left) and fraction of the energy loss to incident energy of cosmic ray muons as a function of initial muon energy using Geant4 and Bethe equation (right).

5. Results

5.1. Geant4 simulations

Various mono-energetic muons are generated to evaluate a functionality of our proposed Cherenkov muon spectrometer in Geant4 simulations. Measured photon signals are classified into two categories, Cherenkov photons (signals) and others (noise). In Geant4 simulations, three mono-energetic muons, $p_\mu = 0.5, 3.1$ and 10.0 GeV/c, horizontally enter Cherenkov muon spectrometer and travel through all radiators as shown in Fig. 10. When $p_\mu = 0.5$ GeV/c, only the first radiator emits Cherenkov radiation because muon momentum is greater than the threshold momentum of first radiator. Similarly, the first four and all radiators emit conical-shaped Cherenkov radiation when $p_\mu = 3.1$ and 10.0 GeV/c, respectively. In addition to Cherenkov light, scintillation photons are observed in some radiators as shown in Fig. 10 even when $p_\mu < p_{th}$. Scintillation photons can be efficiently discriminated from Cherenkov radiation using (i) characteristic photon emission direction (θc vs 4π) and (ii) light flash timing, and (iii) photon emission spectrum. Furthermore, a scintillation photon yield is not significant in all radiators except solid radiator. No transition radiation is observed in Fig. 10 because it is a highly rare event for a few GeV muons and for the small number of boundary system.

It is noteworthy that a negatively charged particle production (a trajectory in red except a muon) in the second radiator is observed in Fig. 10-(c). Optical photons occur due to either Compton scattering or Cherenkov photon emissions by secondary particles, mainly electrons, which can be produced by radiative muon decays and muon to electron conversions [55]:

$$\mu^- \rightarrow e^- \bar{\nu}_e \nu_\mu \quad (19)$$

$$\mu N_{Al} \rightarrow e N_{Al} \quad (20)$$

Eq. (19) represents a radiative decay of μ^- with a mean lifetime of $\tau_\mu \cong 2.2 \mu\text{sec}$. Radiative muon decays are a primary source of secondary charged particles, electrons. Eq. (20) represents a muon to electron conversion ($\mu \rightarrow e$). Muons can be captured by the $1s$ orbital of aluminum, then mono-energetic electron emits with an absence of neutrino [56].

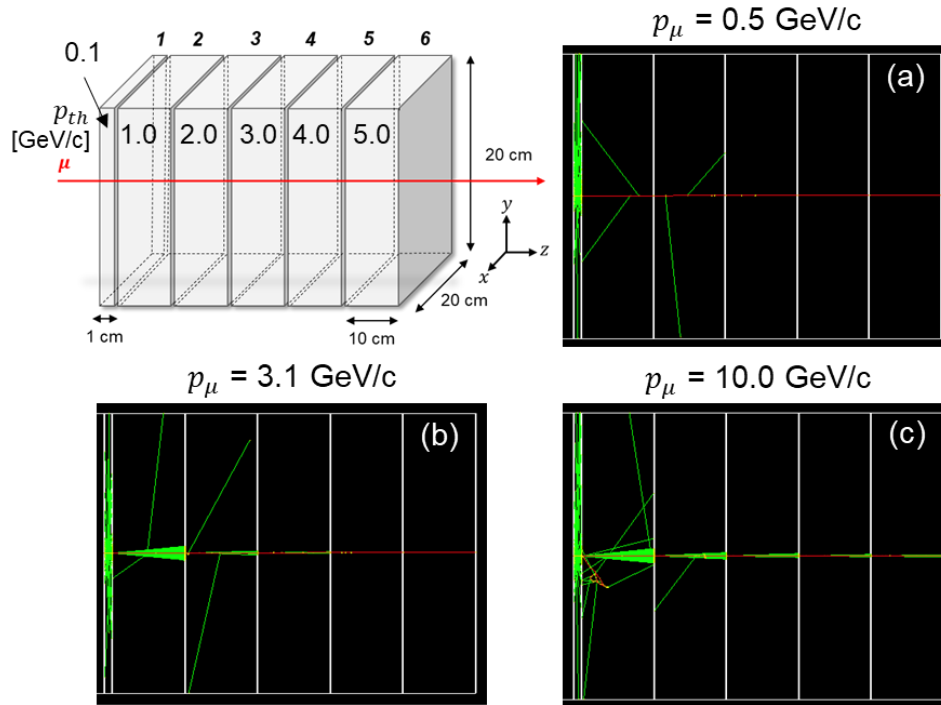


Fig. 10. Overview of Cherenkov muon spectrometer and visualized Geant4 simulations when a single negatively charged muon horizontally enters in the center. Three mono-energy muons are simulated: (a) $p_\mu = 0.5 \text{ GeV}/c$, (b) $p_\mu = 3.1 \text{ GeV}/c$, and (c) $p_\mu = 10.0 \text{ GeV}/c$. Cherenkov radiation is observed only when muon momentum exceeds a threshold momentum level of radiators. Unlike Cherenkov radiation, scintillation photons are emitted in all directions. Secondary particle (e^-) is also observed in (c) due to either a muon radiative decay or muon to electron conversion. Note: red and green represent negatively charged particles and photons, respectively.

5.2. Performance evaluation

We evaluated the performance of our proposed Cherenkov muon spectrometer by reconstructing a sea-level cosmic ray muon spectrum. Analytical models and experimental results of a cosmic ray muon spectrum at sea level can be found in literature [57–59]. We used an open-source Monte Carlo muon generator (“Muon_generator_v3” [60]) which is developed based on semi-empirical model by Smith and Duller [61]. The result of reconstructed cosmic ray muon spectrum using six momentum groups is shown in Fig. 11. The last bin in histogram shows a disagreement with the actual cosmic ray muon spectrum because all muons that have momentum greater than 5.0 GeV/c are categorized in “>5.0 GeV/c” bin. This maximum measurable momentum level problem can be resolved by extending the threshold momentum range and increasing the number of radiators. However, although the increased number of radiators within

a limited overall size improves momentum measurement resolution, it will negatively impact the SNR and degrade the measurement quality (accuracy) due to decreased Cherenkov photon signals in each radiator. In other words, the optimal number of radiators is a balance between two tradeoffs and it must be selected in accordance with conditions such as required size, resolution, and accuracy.

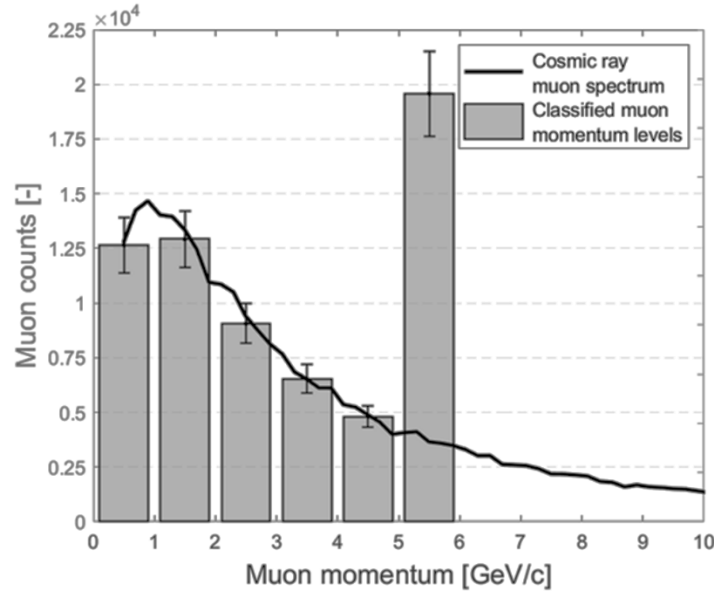


Fig. 11. Reconstructed cosmic ray muon spectrum using the proposed Cherenkov spectrometer with six radiators. Error bars represents 1σ .

5.3. Classification rate

To evaluate the accuracy of our proposed Cherenkov muon spectrometer, a concept of classification rate (CR) is described. It represents the probability that a momentum estimator from signal readout correctly indicates the actual muon momentum range:

$$CR = \frac{\text{True Positive Classification}}{\text{Positive Classification}} \quad (21)$$

where Positive Classification represents the recorded muon counts in a certain momentum class and True Positive Classification represents the expected muon counts when actual incoming muon momenta are given. Geant4 simulation results for optical photon signal responses from all radiators when $p_\mu = 1.1$ and 3.1 GeV/c ($N_\mu = 10^4$) are shown in Fig. 12. A significant difference in photon counts between when $p_\mu > p_{th}$ and $p_\mu < p_{th}$ is observed and it can be utilized to estimate actual muon momentum by analyzing photon signals from each radiator. However, due to a presence of noise, the expected number of optical photons for all radiators (SiO₂ and five pressurized CO₂) are non-zero even when $p_\mu = 1.1$ GeV/c. Because noise signals in undesirable radiators, e.g., scintillation and Cherenkov radiation by secondary particles, are much smaller than primary Cherenkov radiation signals, we can filter them out by deducting a certain level of counts from total photon signals, a technique also known as signal discriminator. The use of both signal

discriminator levels of 1 and 2 to eliminate noise signal when $p_\mu = 1.1$ and 3.1 GeV/c is shown in Fig. 12. In both examples, noise signals are efficiently removed by a level-2 discriminator.

Further, an analysis of the classification rate for muon momentum range from 0.1 to 10.0 GeV/c is performed using 10^4 mono-energetic muon samples in Geant4 simulations. The results are shown in Fig. 13. In the low muon momentum range (< 1.0 GeV/c), CR is $70\text{--}80\%$ with a level-2 discriminator due to strong scintillation photon signals in the glass radiator. In the intermediate momentum range ($1.0 < p_{th} < 7.0$ GeV/c), the discriminator plays a significant role to maintain the CR level greater than 90% . In the high momentum range ($7.0 < p_{th} < 10.0$ GeV/c), however, the CR level decreases because the Cherenkov photon intensity is too low in rarefied CO_2 gas radiators (approximately < 0.5 atm). Therefore, using a discriminator must be avoided in this range. When a combination of various discriminator levels is applied, i.e., a level-2 discriminator for low and intermediate momentum ranges, level 0 or 1 for a high momentum range, then we can achieve a mean classification rate of 90.08% . The classification rate can be further increased using additional signal processing techniques, e.g., timing discrimination.

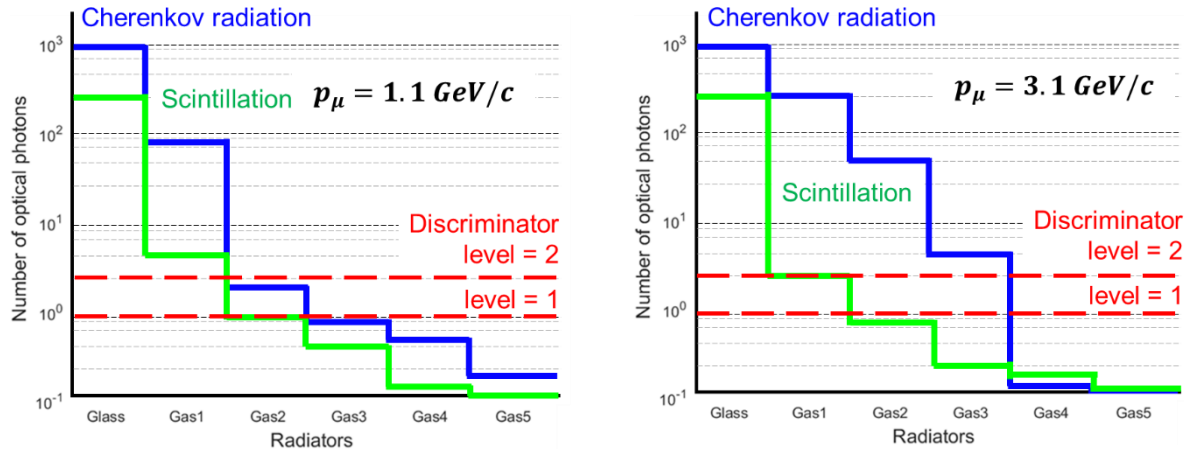


Fig. 12. Geant4 simulation results for optical photon signals from all radiators (SiO_2 and five pressurized CO_2) when $p_\mu = 1.1$ (left) and 3.1 GeV/c (right) ($N_\mu = 10^4$). A noticeable difference in photon counts between when $p_\mu > p_{th}$ and $p_\mu < p_{th}$ is observed. The use of both signal discriminator levels of 1 and 2 to eliminate noise signal is also presented.

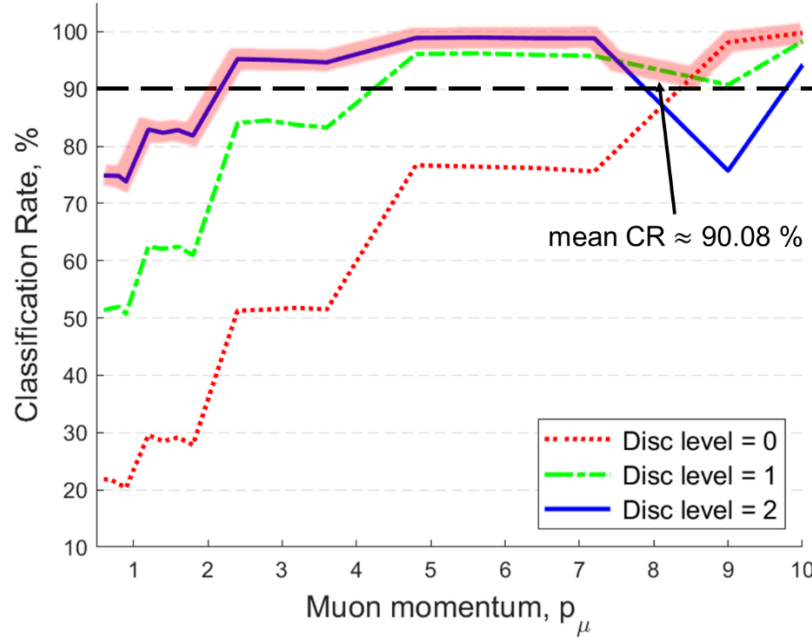


Fig. 13. Geant4 simulation results for classification rates of proposed Cherenkov muon spectrometer as a function of muon momentum from 0.1 to 10.0 GeV/c using 10^4 muons. Various signal discriminator levels are used to minimize noise signals. A mean CR using a combination of discriminator level of 0, 1, and 2 is 90.08 % (highlighted plot).

6. Conclusion

In this paper, we presented a new concept for muon momentum measurement using multiple pressurized gas Cherenkov radiators and performed a detailed feasibility study using analytical models and Geant4 Monte-Carlo muon transport simulations. To eliminate the need for magnetic or time-of-flight spectrometers, our muon spectrometer relies on pressurized gas Cherenkov radiators. In this work, six sequential threshold momentum levels were selected, 0.1, 1.0, 2.0, 3.0, 4.0, and 5.0 GeV/c. When a muon passes all radiators, none to all Cherenkov radiators can emit Cherenkov radiation depending on the actual muon momentum. By monitoring photon signal readout from optical sensors in each radiator, we can find out radiators that emit Cherenkov radiation. Then, we can estimate the actual muon momentum by analyzing digital signals from radiators with a designed momentum resolution.

Our results demonstrate that muon momentum can be estimated with a resolution of ± 0.5 GeV/c using 6 radiators, one SiO_2 and five pressurized CO_2 , over the range of 0.1 to 5.0 GeV/c. Despite the presence of various noise sources, e.g., scintillation, transition radiation, and secondary particles (mainly electrons), we successfully classified the actual muon momentum by analyzing recorded photon signals. To improve measurement accuracy, a signal discriminator is devised to efficiently eliminate noise from signals. The performance of our proposed muon spectrometer was evaluated using classification rate over muon momentum range from 0.1 to 10.0 GeV/c. The results showed a mean classification rate of approximately 90.08 %. The performance of our Cherenkov muon spectrometer can be further improved by applying additional techniques to discriminate scintillation from Cherenkov radiation, e.g., timing discrimination. Finally, the momentum measurement resolution and the momentum range can be improved by increasing the number of radiators.

CRedit authorship contribution statement

J. Bae: Resource, Methodology, Supervision, Numerical and analytical computation, Writing – original draft. **S. Chatzidakis:** Investigation, Supervision, Project administration, Funding acquisition, Writing – review & editing.

Declaration of competing interest

The authors declare that they have no known competing financial interests or personal relationships that could have appeared to influence the work reported in this paper.

Data availability

The data that support the findings of this study are available from the corresponding author upon reasonable request.

Acknowledgments

This research is being performed using funding from the Purdue Research Foundation.

References

- [1] Z. Djurcic, Backgrounds in neutrino appearance signal at MiniBooNE, AIP Conf. Proc. 842 (2006) 828–830.
- [2] E. Twedt, Search for heavy neutrinos at the CMS detector, AIP Conf. Proc. 1200 (2009) 888–891.
- [3] S. Chatzidakis, L.H. Tsoukalas, Investigation of Imaging Spent Nuclear Fuel Dry Casks Using Cosmic Ray Muons, Trans. Am. Nucl. Soc. (2016) 152–155.
- [4] J. Durham, E. Guardincerri, C. Morris, D. Poulson, J. Bacon, D. Chichester, J. Fabritius, S. Fellows, K. Plaud-Ramos, D. Morley, P. Winston, Cosmic Ray Muon Imaging of Spent Nuclear Fuel in Dry Storage Casks, J. Nucl. Mater. Manag. 44 (2016).
- [5] S. Chatzidakis, C.K. Choi, L.H. Tsoukalas, Analysis of Spent Nuclear Fuel Imaging Using Multiple Coulomb Scattering of Cosmic Muons, IEEE Trans. Nucl. Sci. 63 (2016) 2866–2874.
- [6] G. Jonkmans, V.N.P. Anghel, C. Jewett, M. Thompson, Nuclear waste imaging and spent fuel verification by muon tomography, Ann. Nucl. Energy. 53 (2013) 267–273.
- [7] D. Poulson, J.M. Durham, E. Guardincerri, C.L. Morris, J.D. Bacon, D. Morley, A.A. Hecht, Cosmic ray muon computed tomography of spent nuclear fuel in dry storage casks, Nucl. Inst. Methods Phys. Res. A. 842 (2017) 48–53.
- [8] O. Kamaev, E.T. Rand, B.M. Van Der Ende, M. Thompson, S. Livingstone, V. V Golovko, Complementary non-destructive detection of nuclear materials with passive neutron and gamma-ray detectors, and a large-volume muon tomography system, Nucl. Inst. Methods Phys. Res. A. 944 (2019).

- [9] V. Anghel, J. Armitage, J. Botte, K. Boudjemline, D. Bryman, E. Charles, T. Cousins, A. Erlandson, G. Gallant, C. Jewett, G. Jonkmans, Z. Liu, S. Noel, G. Oakham, T.J. Stocki, M. Thompson, D. Waller, Cosmic Ray Muon Tomography System Using Drift Chambers for the Detection of Special Nuclear Materials, *IEEE NSS MIC*. (2010) 547–551.
- [10] K. Gnanvo, L. V Grasso, M. Hohlmann, J.B. Locke, A. Quintero, D. Mitra, Imaging of high- Z material for nuclear contraband detection with a minimal prototype of a muon tomography station based on GEM detectors, *Nucl. Inst. Methods Phys. Res. A*. 652 (2011) 16–20.
- [11] S. Pesente, S. Vanini, M. Benettoni, G. Bonomi, P. Calvini, P. Checchia, E. Conti, F. Gonella, G. Nebbia, S. Squarcia, G. Viesti, A. Zenoni, G. Zumerle, First results on material identification and imaging with a large-volume muon tomography prototype, *Nucl. Inst. Methods Phys. Res. A*. 604 (2009) 738–746.
- [12] L.J. Schultz, K.N. Borozdin, J.J. Gomez, G.E. Hogan, J.A. McGill, Image reconstruction and material Z discrimination via cosmic ray muon radiography, *Nucl. Instruments Methods Phys. Res. A*. 519 (2004) 687–694.
- [13] M. Hohlmann, P. Ford, K. Gnanvo, J. Helsby, D. Pena, R. Hoch, A.C. Ray, M. Generator, GEANT4 Simulation of a Cosmic Ray Muon Tomography System With Micro-Pattern Gas Detectors for the Detection of High- Z Materials, *IEEE Trans. Nucl. Sci.* 56 (2009) 1356–1363.
- [14] J. Bae, S. Chatzidakis, Momentum-Dependent Cosmic Ray Muon Computed Tomography Using a Fieldable Muon Spectrometer, *Energies*. 15 (2022). <https://doi.org/10.3390/en15072666>.
- [15] D. Schouten, P. Ledru, Muon Tomography Applied to a Dense Uranium Deposit at the McArthur River Mine, *J. Geophys. Res. Solid Earth*. 123 (2018) 8637–8652.
- [16] E. Guardincerri, C. Rowe, E. Schultz-Fellenz, M. Roy, N. George, C. Morris, J. Bacon, M. Durham, D. Morley, K. Plaud-Ramos, D. Poulson, D. Baker, A. Bonneville, R. Kouzes, 3D Cosmic Ray Muon Tomography from an Underground Tunnel, *Pure Appl. Geophys.* 174 (2017) 2133–2141.
- [17] H.K.M. Tanaka, H. Taira, T. Uchida, M. Tanaka, M. Takeo, T. Ohminato, Y. Aoki, R. Nishitama, D. Shoji, Three - dimensional computational axial tomography scan of a volcano with cosmic ray muon radiography, *J. Geophys. Res.* 115 (2010) 1–9.
- [18] J. Marteau, D. Gibert, N. Lesparre, F. Nicollin, P. Noli, F. Giacoppo, Muons tomography applied to geosciences and volcanology, *Nucl. Inst. Methods Phys. Res. A*. 695 (2012) 23–28.
- [19] N. Lesparre, D. Gibert, J. Marteau, D. Carbone, E. Galichet, Geophysical muon imaging: feasibility and limits, *Geophys. J. Int.* 183 (2010) 1348–1361.
- [20] R. Kouzes, A. Bonneville, A. Lintereur, A. Mahrous, I. Mostafanezhad, Novel Muon Tomography Detector for the Pyramids, *IEEE Nucl. Sci. Symp. Med. Imaging Conf.* (2021).
- [21] K. Morishima, M. Kuno, A. Nishio, N. Kitagawa, Y. Manabe, M. Moto, F. Takasaki, H. Fujii, K. Satoh, H. Kodama, K. Hayashi, S. Odaka, S. Procureur, D. Attié, S. Bouteille, D. Calvet, C. Filosa, P. Magnier, I. Mandjavidze, M. Riallot, B. Marini, P. Gable, Y. Date, M. Sugiura, Y. Elshayeb, T. Elnady, M. Ezzy, E. Guerriero, Discovery of a big void in Khufu’s Pyramid by observation of cosmic-ray muons, *Nature*. 386–390 (2017) 4–14.
- [22] M. Iodice, Micromegas detectors for the Muon Spectrometer upgrade of the ATLAS experiment, *J. Instrum.* 10 (2015).
- [23] M. Boezio, V. Bonvicini, P. Schiavon, A. Vacchi, N. Zampa, Energy spectra of atmospheric

- muons measured with the CAPRICE98 balloon experiment, *Phys. Rev. D.* 6 (2003) 1–15.
- [24] M. Antonello, B. Baibussinov, V. Bellini, P.A. Benetti, F. Boffelli, A. Bubak, E. Calligarich, S. Centro, T. Cervi, A. Cesana, K. Cieslik, A.G. Cocco, A. Dabrowska, A. Dermenev, A. Falcone, C. Farnese, A. Fava, A. Ferrari, D. Gibin, S. Gninenko, A. Guglielmi, M. Haranczyk, J. Holeczek, M. Janik, M. Kirsanov, J. Kisiel, I. Kochanek, J. Lagoda, A. Menegolli, G. Meng, C. Montanari, S. Otwinowski, P. Picchi, F. Pietropaolo, P. Plonski, A. Rappoldi, G. Raselli, M. Rossella, C. Rubbia, P. Sala, A. Scaramelli, F. Sergiampietri, M. Spanu, D. Stefan, R. Sulej, M. Szarska, M. Terrani, M. Torti, F. Tortorici, F. Varanini, S. Ventura, C. Vignoli, H. Wang, X. Yang, A. Zalewskag, A. Zani, K. Zaremba, Muon momentum measurement in ICARUS-T600 LAr-TPC via multiple scattering in few-GeV range, *J. Instrum.* 12 (2017).
- [25] O.C. Allkofer, R.D. Andresen, W.D. Dau, The muon spectra near the geomagnetic equator, *Can. J. Phys.* 46 (1968) 301–305.
- [26] J. Bae, S. Chatzidakis, A New Semi-Empirical Model for Cosmic Ray Muon Flux Estimation, *Prog. Theor. Exp. Phys.* 2022 (2022). <https://doi.org/10.1093/ptep/ptac016>.
- [27] J. Bae, S. Chatzidakis, R. Bean, Effective Solid Angle Model and Monte Carlo Method: Improved Estimations to Measure Cosmic Muon Intensity at Sea Level in All Zenith Angles, *Int. Conf. Nucl. Eng.* (2021).
- [28] S. Chatzidakis, P.A. Hausladen, S. Croft, J.A. Chapman, J.J. Jarrell, J.M. Scaglione, C.K. Choi, L.H. Tsoukalas, Exploring the Use of Muon Momentum for Detection of Nuclear Material Within Shielded Spent Nuclear Fuel Dry Casks, *Am. Nucl. Soc. Annu. Meet.* (2017) 190–193.
- [29] J. Bae, S. Chatzidakis, The Effect of Cosmic Ray Muon Momentum Measurement for Monitoring Shielded Special Nuclear Materials, *INMM/ESARDA Jt. Annu. Meet.* (2021).
- [30] J. Bae, S. Chatzidakis, Fieldable Muon Momentum Measurement using Coupled Pressurized Gaseous Cherenkov Detectors, *Trans. Am. Nucl. Soc.* 125 (2021) 400–403.
- [31] P.A. Cherenkov, Visible emission of clean liquids by action of gamma radiation, *Dokl. Akad. Nauk SSSR.* 2 (1934).
- [32] H. Kragh, The Lorenz-Lorentz Formula : Origin and Early History, *Substantia.* 2 (2018) 7–18.
- [33] J. V. Jelley, Čerenkov radiation: Its origin, properties and applications, *Contemp. Phys.* 3 (1961) 45–57.
- [34] G. Neil, Thomas Jefferson National Accelerator Facility FEL Industrial Applications, in: *Jt. Accel. Conf.*, 1998: pp. 88–92.
- [35] A.H. Harvey, E. Paulechka, P.F. Egan, Candidates to replace R-12 as a radiator gas in Cherenkov detectors, *Nucl. Instruments Methods Phys. Res. Sect. B.* 425 (2018) 38–42.
- [36] M. Richter, M.O. Mclinden, E.W. Lemmon, Thermodynamics Properties of 2,3,3,3-Tetrafluoroprop-1-ene (R1234yf): Vapor Pressure and p-p-T Measurement and an Equation of State, *J. Chem. Eng. Data.* 56 (2011) 3254–3264.
- [37] D.J. Hayes, Cherenkov Detectors at Jefferson Lab, College of William and Mary, 2018.
- [38] Geant4 Collaboration, *Physics Reference Manual (Release 10.4)*, 2017.
- [39] I. Frank, I. Tamm, Coherent visible radiation of fast electrons passing through matter, *Comptes Rendus Acad. Sci.* (1937).

- [40] J. V. Jelley, Čerenkov Radiation and its Applications, 1958.
- [41] D.L. Burden, G.M. Hieftje, Čerenkov Radiation as a UV and Visible Light Source for Time-Resolved Fluorescence, *Am. Chem. Soc.* 70 (1998) 3426–3433.
- [42] G.F. Knoll, *Radiation Detection and Measurement*, 4th ed., Wiley, 2010.
- [43] J.B. Birks, Scintillations from Organic Crystals: Specific Fluorescence and Relative Response to Different Radiations, *Proc. Phys. Soc. Sect. A.* 64 (1951) 874–877.
- [44] H.A. Bethe, Molière’s Theory of Multiple Scattering, *Phys. Rev.* 89 (1953) 1256–1266.
- [45] B. Bengtson, M. Moszynski, Energy-transfer and Light-collection Characteristics for Different Types of Plastic Scintillators, *Nucl. Instruments Methods.* 117 (1974) 227–232.
- [46] T. Kaptanoglu, M. Luo, J. Kelin, Čerenkov and scintillation light separation using wavelength in LAB based liquid scintillator, *J. Instrum.* 14 (2019).
- [47] J. Bae, S. Chatzidakis, Fieldable muon spectrometer using multi-layer pressurized gas Čerenkov radiators and its applications, *Sci. Rep.* 12 (2022). <https://doi.org/https://doi.org/10.1038/s41598-022-06510-2>.
- [48] John David Jackson, *Classical Electrodynamics*, Wiley, 1962.
- [49] F. Sakamoto, H. Iijima, K. DOBASHI, T. IMAI, T. UEDA, T. WATANABE, M. UESAKA, Emittance and Energy Measurements of Low- Energy Electron Beam Using Optical Transition Radiation Techniques, *Jpn. J. Appl. Phys.* 44 (2005) 1485–1491.
- [50] J. Bae, *A Novel Muon Spectrometer Using Multi-Layer Pressurized Gas Čerenkov Radiators for Muon Tomography*, Purdue University, 2022.
- [51] S. Agostinelli, J. Allison, K. Amako, J. Apostolakis, H. Araujo, P. Arce, M. Asai, D. Axen, S. Banerjee, G. Barrand, F. Behner, L. Bellagamba, J. Boudreau, L. Broglia, A. Brunengo, H. Burkhardt, S. Chauvie, J. Chuma, R. Chytracsek, G. Cooperman, G. Cosmo, P. Degtyarenko, A. Dell’Acqua, G. Depaola, D. Dietrich, R. Enami, A. Feliciello, C. Ferguson, H. Fesefeldt, G. Folger, F. Foppiano, A. Forti, S. Garelli, S. Giani, R. Giannitrapani, D. Gibin, J.J. Gomez Cadenas, I. Gonzalez, G. Gracia Abril, G. Greeniaus, W. Greiner, V. Grichine, A. Grossheim, S. Guatelli, P. Gumplinger, R. Hamatsu, K. Hashimoto, H. Hasui, A. Heikkinen, A. Howard, V. Ivanchenko, A. Johnson, F.W. Jones, J. Kallenbach, N. Kanaya, M. Kawabata, Y. Kawabata, M. Kawaguti, S. Kelner, P. Kent, A. Kimura, T. Kodama, R. Kokoulin, M. Kossov, H. Kurashige, E. Lamanna, T. Lampen, V. Lara, V. Lefebure, F. Lei, M. Liendl, W. Lockman, F. Longo, S. Magni, M. Maire, E. Medernach, K. Minamimoto, P. Mora de Freitas, Y. Morita, K. Murakami, M. Nagamatu, R. Nartallo, P. Nieminen, T. Nishimura, K. Ohtsubo, M. Okamura, S. O’Neale, Y. Oohata, K. Paech, J. Perl, A. Pfeiffer, M.G. Pia, F. Ranjard, A. Rybin, S. Sadilov, E. di Salvo, G. Santin, T. Sasaki, N. Savvas, Y. Sawada, S. Scherer, S. Sei, V. Sirotenko, D. Smith, N. Starkov, H. Stoecker, J. Sulkimo, M. Takahata, S. Tanaka, E. Tcherniaev, E. Safai Tehrani, M. Tropeano, P. Truscott, H. Uno, L. Urban, P. Urban, M. Verderi, A. Walkden, W. Wander, H. Weber, J.P. Wellisch, T. Wenaus, D.C. Williams, D. Wright, T. Yamada, H. Yoshida, D. Zschesche, GEANT4 - A simulation toolkit, *Nucl. Instruments Methods Phys. Res. Sect. A Accel. Spectrometers, Detect. Assoc. Equip.* 506 (2003) 250–303.
- [52] J. Allison, K. Amako, J. Apostolakis, H. Araujo, P.A. Dubois, M. Asai, G. Barrand, R. Capra, S. Chauvie, R. Chytracsek, G.A.P. Cirrone, G. Cooperman, G. Cosmo, G. Cuttone, G.G. Daquino, M. Donszelmann, M. Dressel, G. Folger, F. Foppiano, J. Generowicz, V. Grichine, S. Guatelli, P. Gumplinger, A. Heikkinen, I. Hrivnacova, A. Howard, S. Incerti, V. Ivanchenko, T. Johnson, F.

- Jones, T. Koi, R. Kokoulin, M. Kossov, H. Kurashige, V. Lara, S. Larsson, F. Lei, F. Longo, M. Maire, A. Mantero, B. Mascialino, I. McLaren, P.M. Lorenzo, K. Minamimoto, K. Murakami, P. Nieminen, L. Pandola, S. Parlati, L. Peralta, J. Perl, A. Pfeiffer, M.G. Pia, A. Ribon, P. Rodrigues, G. Russo, S. Sadilov, G. Santin, T. Sasaki, D. Smith, N. Starkov, S. Tanaka, E. Tcherniaev, B. Tomé, A. Trindade, P. Truscott, L. Urban, M. Verderi, A. Walkden, J.P. Wellisch, D.C. Williams, D. Wright, H. Yoshida, M. Peirgentili, Geant4 developments and applications, *IEEE Trans. Nucl. Sci.* 53 (2006) 270–278.
- [53] V.L. Highland, Some practical remarks on multiple scattering, *Nucl. Instruments Methods.* 129 (1975) 497–499.
- [54] P.A. Zyla et al., *The Review of Particle Physics (2020)*, *Prog. Theor. Exp. Phys.* (2020).
- [55] R. Donghia, The Mu2e experiment at Fermilab : Design and status, *NUOVO Cim.* 40C (2017) 1–7.
- [56] R.P. Litchfield, Status of the AICap experiment, in: *Proc. Sci.*, 2014.
- [57] P.K.F. Grieder, *Cosmic Rays at Earth*, in: Elsevier Sci., Elsevier Science, 2001.
- [58] T. K. Gaisser et al, *Cosmic rays and particle physics*, Cambridge University Press, 2016.
- [59] B. Rossi, *Cosmic Rays*, McGraw-Hill Book Company, 1964.
- [60] S. Chatzidakis, S. Chrysikopoulou, L.H. Tsoukalas, M. Carlo, Developing a cosmic ray muon sampling capability for muon tomography and monitoring applications, *Nucl. Inst. Methods Phys. Res. A.* 804 (2015) 33–42.
- [61] J.A. Smith, N.M. Duller, Effects of pi meson decay-absorption phenomena on the high-energy mu meson zenithal variation near sea level, *J. Geophys. Res.* 64 (1959) 2297–2305.